Journal of Sound and Vibration (1999) **222**(2), 191–207
Article No. jsvi.1998.2007, available online at http://www.idealibrary.com.on IDEAL

CONFIGURATION DEPENDENT EIGENFREQUENCIES FOR A TWO-LINK FLEXIBLE MANIPULATOR: EXPERIMENTAL VERIFICATION

R. I. MILFORD

Hughes Space & Communications Company, *El Segundo*, *CA* 90245, *USA*

AND

S. F. ASOKANTHAN

Department of Mechanical Engineering, *University of Queensland*, *St Lucia*, *Qld* 4072, *Australia*

(*Received* 18 *November* 1997, *and in final form* 24 *September* 1998)

In this paper, the exact partial differential equations governing the system modes of a general two-link flexible manipulator are derived by matching the boundary equations at the elbow. The resulting partial differential equation formulation is solved numerically to yield the exact eigenfrequencies corresponding to arbitrary elbow angles. The eigenfrequencies are shown to be a strong function of manipulator configuration, varying by up to 30% as the manipulator sweeps across its range of motion; this is subsequently shown to accurately predict the eigenfrequencies of an experimental two-link manipulator.

1. INTRODUCTION

In this paper, the eigenfrequencies of a two-link flexible robot manipulator with a locked elbow are derived analytically by formulation and solution of the exact partial differential equations (PDEs). Accurate modelling is required for the synthesis of high bandwidth vibration controllers, and is made challenging by the parametric sensitivity of the structural dynamics, particularly to load and configuration which typically vary during operation. While accurate models can be easily developed using finite element methods, parametric methods such as assumed modes (see, e.g., reference [1]) are useful in providing a better physical understanding of the problem.

The modal characteristics of many simple distributed beam structures with concentrated mass and spring elements have been well documented (see, e.g., reference [2]). A number of researchers have examined single and two-link manipulators for robotic applications. Schmitz [3] developed the unconstrained modal analysis of a pinned–free beam taking into account the hub inertia and

0022–460X/99/170191 + 17 $30.00/0

payload mass, but neglected to include the rotary inertia of the tip mass. This model has become the *de facto* model for a number of researchers (see, e.g., reference [4]). However, for high hub inertias which result in a near fixed or cantilevered boundary condition, the model becomes invalid as the modal slope vanishes at the joint, and is therefore only applicable to manipulators with high beam-to-hub coupling or "near-pinned" joints.

Barbieri and Ozguner [5] investigated the use of both *constrained* and *unconstrained* mode shapes for open-loop modelling of a single-link to span the full range of hub inertias. Up to this point, researchers had neglected the open-loop servo dynamics and the effect of closed-loop collocated feedback control on mode shapes. Garcia and Inman [6] addressed the effect of servo dynamics and control on the dynamics of the complete structure, and highlighted the fact that the mode shapes were dependent on the feedback control.

Oakley and Cannon [7] developed the dynamic equations for a general two-link manipulator including geometric offsets and all concentrated inertias. Global or system modes were used to describe the total mode shapes of the structure instead of the more common component modes for each link, however, the boundary equations at the elbow were approximated and servo dynamics were neglected. In addition, the actual eigenfunctions used were *admissible component* mode (i.e., for each link) functions based on the boundary conditions for a cantilever with a tip inertia which do not fully satisfy the boundary conditions of the elbow joint. Increased accuracy was obtained by incorporating the approximate eigenfunctions into an exact dynamic formulation from which the system modes could be recalculated as a weighted combination of admissible mode shapes.

In this paper, exact PDEs and boundary equations of a two-link flexible manipulator system are obtained by matching the shear force and bending moment at the elbow joint, allowing the eigenvalues to be computed without recourse to dynamic formulations. The paper begins with a definition of the two-link manipulator system to be modelled followed by the modal analysis and concludes with the presentation and comparison of analytical and experimental results. Servo actuator effects on the boundary equations of the PDEs are addressed in the appendix.

2. TWO-LINK MANIPULATOR PHYSICAL MODEL

A model of a planar two-link flexible manipulator is illustrated in Figure 1. The system is composed of two links, each with a revolute joint powered by a DC servo-motor, and a flexible beam. The first link is referred to as the upper arm and the second as the lower arm (or *forearm*). Similarly the first joint is referred to as the *shoulder* and the second joint as the *elbow*. The tip of the forearm link is the end-point of the manipulator which normally carries a gripper. The manipulator is a representation of the major structural characteristics of space telerobotic manipulators.

The following definitions apply to the parameters shown in Figure 1 and define all of the material and geometric parameters required for modal analysis. Each link is referenced by the subscript $l = 1, 2$, numbered sequentially from the

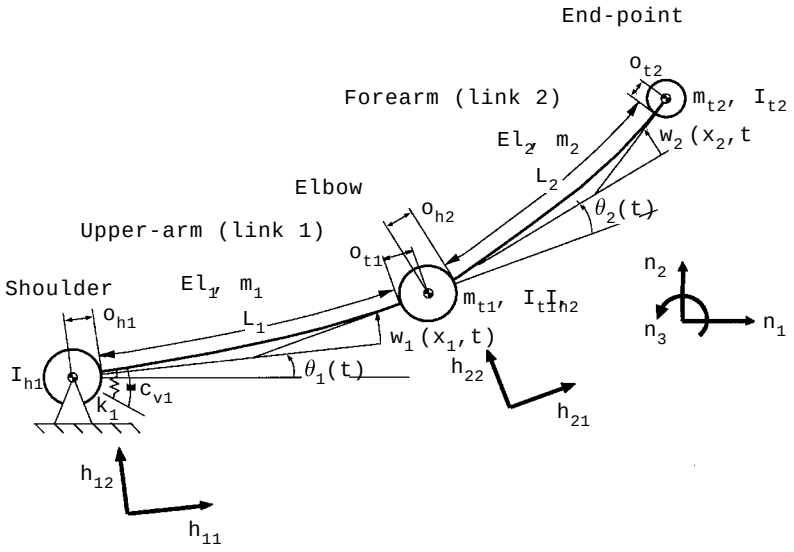

Figure 1. Two-link manipulator model.

shoulder: EI_l, flexural rigidity; m_l, mass per unit length; L_l, length; $\theta_l(t)$, rigid hub angle; x_l, distance along the undeflected neutral axis; $w_l(x_l, t)$, transverse elastic deflection of the flexible link; I_{hl}, hub inertia; I_{tl}, tip inertia; m_{tl}, tip mass; m_{bl}, beam mass; c_{vl}, viscous friction; k_l, joint stiffness (electromechanical); o_{hl}, o_{tl}, the distance between the axis of rotation and the beam attachment for the hub and tip of link l (i.e., geometric offsets).

For simplicity, the elbow is treated as "locked", hence the stiffness and damping for the elbow joint have been omitted from Figure 1. The geometric offsets are measured axially along the undeflected beam neutral axis, with transverse offsets assumed to be negligible. The axis of rotation and the centre of gravity for each rigid hub are assumed to be coincident. A global co-ordinate system is defined by the fixed basis **n**, and two rotating co-ordinate systems are affixed to the shoulder hub and elbow hub and defined by ($\mathbf{h}_{11}$, $\mathbf{h}_{12}$) and ($\mathbf{h}_{21}$, $\mathbf{h}_{22}$), respectively.

In the ensuing analysis, the joints of the manipulator are assumed to be stiff in comparison with the links. Additionally, gravity is neglected since the focus is on space manipulators which operate in a low gravity environment. The model in Figure 1 is a representation of the experimental manipulator [8] used to validate the theoretical predictions developed in this paper.

3. MODAL ANALYSIS

3.1. SYSTEM MODES REPRESENTATION

At resonant frequencies, a complex structure vibrates with *global* [9] or *system* [10] mode characteristics, rather than a series of subsystem or *component* modes. Consequently, for a multi-link manipulator it is not strictly correct to formulate the modal deflections in terms of independent *component* mode expansions for each link. However, when approximate *component* modes are incorporated into

a dynamic equation which includes all concentrated mass and inertia terms, the eigenvalues of the dynamic formulation still tend to approach the correct eigenvalues of the system when a large number of modes are retained in the expansion; however, this approach requires the development of a dynamic model before the eigenvalues can be predicted. This is exactly analogous to the use of *admissible* functions instead of true eigenfunctions for a single beam. For a multi-link manipulator or other complex structure, the assumed modes method can be implemented using either *admissible component* modes or the true *system* modes which are the eigenfunctions of the manipulator.

The deflection of each beam is expressed in a *system* mode framework

$$w_l(x_l, t) = \sum_{i=1}^{n} \phi_{li}(x_l) q_i(t), \tag{1}$$

where $w_l(x_l, t)$ is the transverse elastic displacement of the beam from the undeformed neutral axis at position x_l. The shape function $\phi_{li}(x_l)$ represents the ith *system* mode shape component for link l while $q_i(t)$ denotes the ith generalised co-ordinate. Note that a single time dependent co-ordinate describes the entire system for each mode. Consequently the system modes representation contains more information with a lower order model [10]. The deflection $w(x, t)$ along the entire compound "beam" comprising two links is expressed as a linear combination of system mode shapes by

$$w(x, t) = \sum_{i=1}^{n} \Phi_i(x) q_i(t) = \begin{cases} \sum_{i=1}^{n} \phi_{1i}(x_1) q_i(t) & x \leqslant \eta L \\ \sum_{i=1}^{n} \phi_{2i}(x_2) q_i(t) & \eta L < x \leqslant L \end{cases}, \tag{2}$$

where $\phi_{1i}(x_1)$ and $\phi_{2i}(x_2)$ are the two local components of the *global* mode shape $\Phi_i(x)$. The total beam length L is equal to $L_1 + L_2$ and the local axial co-ordinates are defined by

$$0 \leqslant x_1 \leqslant L_1 = \eta L, \qquad 0 \leqslant x_2 \leqslant L_2 = (1 - \eta) L,$$

where $\eta = L_1/(L_1 + L_2)$, $0 < \eta \leqslant 1$ is the length fraction at the elbow joint.

The only practical difference between a model derived using *component* modes and one employing system modes, is that the latter equations are expressed in terms of co-ordinates $q_i(t)$ instead of $q_{1i}(t)$ and $q_{2i}(t)$ producing half the number of modal equations. Once the system mode approach has been adopted however, the choice of eigenfunctions used in equation (1) can range from *component* modes through to the system eigenfunctions, but has no effect on the structure of the formulation, only its accuracy.

Figure 2 defines the co-ordinate system corresponding to the ith system mode for an elbow angle of θ_2 and arbitrary shoulder angle. The elastic deflections are assumed to be transverse with respect to the undeformed neutral axis, and continuity is maintained between the slope and displacement at the end of link 1 and the start of link 2. As a result, the co-ordinate system which is affixed to link

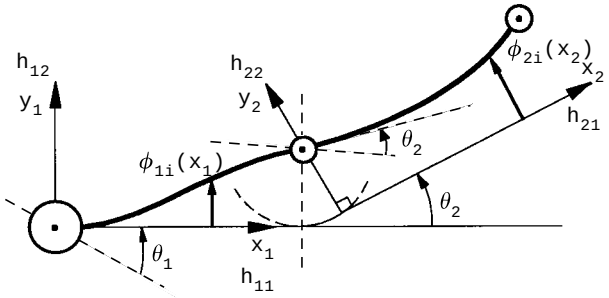

Figure 2. System mode co-ordinate system definition.

2 ($\mathbf{h}_{21}$, $\mathbf{h}_{22}$) is both rotated by θ_2 and translated by $w_1(L_1)$. Joint rotations can be arbitrarily large.

When the exact eigenfunctions are computed, the assumed modes method will exactly model the modal characteristics of the system. It is generally difficult to develop the exact eigenfunctions for a complex structure, which motivated the development of the assumed modes technique, where approximate *admissible* functions may be used. Subsequent refinement of the mode shapes can be accomplished using the eigenfunctions of the final dynamic formulation [10]. This refinement is not required when the true *system* modes are utilized as in the following section.

3.2. DIFFERENTIAL EIGENVALUE PROBLEM

Given a model of the system (Figure 1) and the assumed modes structure (Figure 2), the exact eigenvalues and eigenfunctions can be computed. The differential eigenvalue problem for the above distributed parameter system is described by an infinite dimensional PDE and results in an infinite number of eigenvalues in contrast to the algebraic eigenvalue problem for a finite-dimensional system (see, e.g., reference [1]). It is assumed that the flexible links are slender and that deflections are small compared with their length, so that Euler–Bernoulli beam theory can be used to model the free transverse vibration of the beams. The discontinuity at the elbow requires that two PDEs be used to describe the elastic behaviour of the links [11]

$$EI_l \frac{\partial^4 w_l(x_l, t)}{\partial x_l^4} + m_l \frac{\partial^2 w_l(x_l, t)}{\partial t^2} = 0, \qquad l = 1, 2, \tag{3}$$

which also retains the mass properties of the individual links. The spatial component of the general separation of variables solution (see, e.g., reference [2]) to equation (3) is

$$\phi_{li}(x) = A_{li} \sin(\beta_{li} x_l) + B_{li} \sinh(\beta_{li} x_l) + C_{li} \cos(\beta_{li} x_l) + D_{li} \cosh(\beta_{li} x_l), \tag{4}$$

where $i = 1, 2, \ldots, n$ and $l = 1, 2$. The frequency parameter β_{li} is defined from equation (3) as

$$\beta_{li}^2 = 2\pi f_i \left(\frac{m_l}{EI_l}\right)^{1/2}, \qquad l = 1, 2 \tag{5}$$

for the ith natural frequency f_i and for the first link is related to the eigenvalues through the relation

$$\beta_{1i} = \frac{\lambda_i}{L}. \tag{6}$$

The mode shape constants A_{li}, B_{li}, C_{li} and D_{li} and eigenvalues λ_i are calculated in the sequel.

The geometric offsets shown in Figure 1 are included in the boundary conditions when solving the differential eigenvalue problem, since their effects can be quite significant [10]. Furthermore, the contribution of the rigid-body motion is neglected, since the modal analysis is based on small perturbations about a nominal configuration, in this case $\theta_1 = 0^\circ$ and $\theta_2 = \theta_{20}$, where θ_{20} is the elbow angle about which the system equations are linearised and $\dot{\theta}_1 = \dot{\theta}_2 = 0$. The boundary conditions associated with the constrained structure described by equation (3) are now formulated explicitly from equilibrium relations for displacement, slope, bending moment and shear force denoted respectively by

$$w_l(x_l, t), \qquad \frac{\partial w_l(x_l, t)}{\partial x_l}, \qquad EI_l \frac{\partial^2 w_l(x_l, t)}{\partial x_l^2}, \qquad EI_l \frac{\partial^3 w_l(x_l, t)}{\partial x_l^3}$$

at each of the four beam boundaries (see, e.g., reference [12]). The physical arrangement and the assumptions made are also described for each case. The effect of the DC servomotors on the boundary equations are described in the appendix.

(a) *Joint* 1 (*shoulder*): $x = 0$, $x_1 = 0$

The shoulder joint is modelled as spring-hinged with rotary inertia and a viscous damper [6, 13]

$$w_1(0, t) = 0, \tag{7}$$

$$EI_1 \frac{\partial^2 w_1(x_1, t)}{\partial x_1^2}\bigg|_{x_1 = 0} = k_1 \frac{\partial w_1(x_1, t)}{\partial x_1}\bigg|_{x_1 = 0} + c_{v1} \frac{\partial}{\partial t}\left(\frac{\partial w_1(x_1, t)}{\partial x_1}\bigg|_{x_1 = 0}\right) + I_{h1} \frac{\partial^2}{\partial t^2}\left(\frac{\partial w_1(x_1, t)}{\partial x_1}\bigg|_{x_1 = 0}\right), \tag{8}$$

where k_1 is the equivalent spring stiffness of the joint defined in equation (A3) and c_{v1} is the viscous damping in the joint including the back electro motive force (EMF) and servo rate feedback. Large values of k_1, c_{v1} or I_{h1} all lead to a near-cantilevered boundary condition i.e., $\partial w_1(0, t)/\partial x_1 \Rightarrow 0$, and it is possible to

replace the second natural boundary condition equation (8) with the following geometric boundary condition for a cantilever:

$$\left.\frac{\partial w_1(x_1, t)}{\partial x_1}\right|_{x_1 = 0} = 0.$$

This observation is only noted for potential algebraic simplification since large values of k_1 in equation (8) will result in the same eigenvalues. To retain the generality of the present derivation, this simplification is not made, although the viscous damping term was neglected.

(b) *Joint* 2 (*elbow*): $x = \eta L,\ x_1 = L_1 = \eta L,\ x_2 = 0$

The elbow is spring-hinged like the shoulder, but is treated as locked, to reflect a system with high Coulomb friction and high servo gain. The accuracy of this assumption is demonstrated analytically in the Appendix. Unlike the shoulder joint, the inboard side of the joint is affixed to the end of the first link instead of a rigid support. Thus, the natural boundary conditions are:

$$\begin{aligned} EI_1 \left.\frac{\partial^2 w_1(x_1, t)}{\partial x_1^2}\right|_{x_1 = \eta L} &= EI_2 \left.\frac{\partial^2 w_2(x_2, t)}{\partial x_2^2}\right|_{x_2 = 0} \\ &\quad - (I_{t1} + m_{t1} o_{t1}^2) \frac{\partial^2}{\partial t^2} \left(\left.\frac{\partial w_1(x_1, t)}{\partial x_1}\right|_{x_1 = \eta L} \right) \\ &\quad - m_{t1} o_{t1} \left(\left.\frac{\partial^2 w_1(x_1, t)}{\partial t^2}\right|_{x_1 = \eta L} \right) \\ &\quad - (o_{t1} \cos\theta_2 + o_{h2}) EI_2 \left.\frac{\partial^3 w_2(x_2, t)}{\partial x_2^3}\right|_{x_2 = 0}, \end{aligned} \tag{9}$$

$$\begin{aligned} EI_1 \left.\frac{\partial^3 w_1(x_1, t)}{\partial x_1^3}\right|_{x_1 = \eta L} &= m_{t1} \left[\left.\frac{\partial^2 w_1(x_1, t)}{\partial t^2}\right|_{x_1 = \eta L} \right. \\ &\quad \left. + o_{t1} \frac{\partial^2}{\partial t^2} \left(\left.\frac{\partial w_1(x_1, t)}{\partial x_1}\right|_{x_1 = \eta L} \right) \right] \\ &\quad + EI_2 \left.\frac{\partial^3 w_2(x_2, t)}{\partial x_2^3}\right|_{x_2 = 0} \cos\theta_2 \\ &\quad + (m_{h2} + m_{t2}) \sin^2\theta_2 \left.\frac{\partial^2 w_1(x_1, t)}{\partial t^2}\right|_{x_1 = \eta L}. \end{aligned} \tag{10}$$

Since the joint is not free to rotate, dependence on I_{h2}, c_{v2} and k_2 has been removed from equations (9) and (10). The terms corresponding to the shear force and bending moment from link two would be omitted in a *component* mode development. Extra terms also arise from the elbow angle and offsets. The continuity or geometric boundary conditions for the joint are:

$$w_1(\eta L, t) \cos \theta_2 = w_2(0, t), \tag{11}$$

$$\frac{\partial w_1(x_1, t)}{\partial x_1}\bigg|_{x_1 = \eta L} = \frac{\partial w_2(x_2, t)}{\partial x_2}\bigg|_{x_2 = 0}. \tag{12}$$

(c) *End-point*: $x = L$, $x_2 = L_2 = (1 - \eta)L$

The manipulator end-point is free carrying a concentrated mass with significant rotary inertia:

$$EI_2 \frac{\partial^2 w_2(x_2, t)}{\partial x^2}\bigg|_{x_2 = (1-\eta)L} = -(I_{t2} + m_{t2} o_{t2}^2) \frac{\partial^2}{\partial t^2}\left(\frac{\partial w_2(x_2, t)}{\partial x}\bigg|_{x_2 = (1-\eta)L}\right) - m_{t2} o_{t2} \frac{\partial^2 w_2(x_2, t)}{\partial t^2}\bigg|_{x_2 = (1-\eta)L}, \tag{13}$$

$$EI_2 \frac{\partial^3 w_2(x_2, t)}{\partial x_2^3}\bigg|_{x_2 = (1-\eta)L} = m_{t2} \frac{\partial^2 w_2(x_2, t)}{\partial t^2}\bigg|_{x_2 = (1-\eta)L} + m_{t2} o_{t2} \frac{\partial^2}{\partial t^2}\left(\frac{\partial w_2(x_2, t)}{\partial x}\bigg|_{x_2 = (1-\eta)L}\right). \tag{14}$$

Substituting the expressions for the assumed modes summation for the beam deflection in equation (1) and mode shape functions (4) into the above boundary conditions (7–14), taking Laplace transforms and combining the set of eight homogeneous equations into matrix form, the characteristic equation is obtained as

$$M(\lambda_i)[A_{1i} \quad B_{1i} \quad C_{1i} \quad D_{1i} \quad A_{2i} \quad B_{2i} \quad C_{2i} \quad D_{2i}]^T = 0. \tag{15}$$

The characteristic matrix $M(\lambda)$ is partitioned as

$$M(\lambda) = \begin{bmatrix} M_{11} & M_{12} \\ M_{21} & M_{22} \end{bmatrix}, \tag{16}$$

with submatrices

$$M_{11} = \begin{bmatrix} \epsilon_1\lambda_i^3 - \xi_1/\lambda_i & \epsilon_1\lambda_i^3 - \xi_1/\lambda_i & \{(\cos a_i + \cosh a_i) - \lambda_i^3\alpha_1(\sin a_i + \sinh a_i) \\ \sin a_i + \lambda_i^3\alpha_1 \cos a_i + \eta_1 z_{t1}\lambda_i^2 \sin a_i & -\sinh a_i + \lambda_i^3\alpha_1 \cosh a_i + \eta_1 z_{t1}\lambda_i^2 \sin a_i & +\eta_1 z_{t1}\lambda_i^2 \sin a_i(\cos(a_i) - \cosh(a_i))\} \\ \{-\cos a_i + (z_{mb}\lambda \sin^2\theta_2 + \eta_1\lambda_i)\sin a_i & \{\cosh a_i + (z_{mb}\lambda \sin^2\theta_2 + \eta_1\lambda_i)\sinh a_i & \cdots \quad \{\sin a_i - \sinh a_i + (z_{mb}\lambda \sin^2\theta_2 + \eta_1\lambda_i)(\cos a_i - \cosh a_i) \\ +\eta_1 z_{t1}\lambda_i^2 \cos(a_i)\} & + \eta_1 z_{t1}\lambda_i^2 \cosh(a_i)\} & -\eta_1 z_{t1}\lambda_i^2(\sin(a_i) + \sinh(a_i))\} \end{bmatrix},$$

$$M_{12} = \begin{bmatrix} 0 & 0 & 0 & 0 \\ \Gamma\Gamma'^3(z_{t1}\cos\theta_2 + z_{h2}) & -\Gamma\Gamma'^3(z_{t1}\cos\theta_2 + z_{h2}) & -\Gamma\Gamma'^2 & \Gamma\Gamma'^2 \\ \Gamma\Gamma'^3\cos\theta_2 & -\Gamma\Gamma'^3\cos\theta_2 & 0 & 0 \end{bmatrix},$$

$$M_{21} = \begin{bmatrix} 0 & 0 & 0 \\ 0 & 0 & 0 \\ \cos\theta_2 \sin a_i & \cos\theta_2 \sinh a_i & \cos\theta_2(\cos a_i - \cosh a_i) \\ \cos a_i & \cosh a_i & -(\sin a_i + \sinh a_i) \end{bmatrix}$$

$$M_{22} = \begin{bmatrix} \{-\sin b_i - \alpha_2\Gamma'^3\lambda_i^3 \cos b_i - \eta_2 z_{t2}\Gamma'^2\lambda_i^2 \sin(b_i)\} & \{-\sinh b_i - \alpha_2\Gamma'^3\lambda_i^3 \cosh b_i - \eta_2 z_{t2}\Gamma'^2\lambda_i^2 \sinh(b_i)\} & -\cos b_i + \alpha_2\Gamma'^3\lambda_i^3 \sin b_i - \eta_2 z_{t2}\Gamma'^2\lambda_i^2 \cos(b_i) \\ \{-\cos b_i + \eta_2\Gamma'\lambda_i \sin b_i + \eta_2 z_{t2}\Gamma'^2\lambda_i^2 \cos(b_i)\} & \{-\cosh b_i + \eta_2\Gamma'\lambda_i \sinh b_i + \eta_2 z_{t2}\Gamma'^2\lambda_i^2 \cosh(b_i)\} & \sin b_i + \eta_2\Gamma'\lambda_i \cos b_i - \eta_2 z_{t2}\Gamma'^2\lambda_i^2 \sin(b_i) \\ 0 & 0 & -1 \\ -\Gamma' & -\Gamma' & 0 \end{bmatrix}$$

$$\begin{bmatrix} \cosh b_i - \alpha_2\Gamma'^3\lambda_i^3 \sinh b_i - \eta_2 z_{t2}\Gamma'^2\lambda_i^2 \cosh(b_i) \\ \cdots \quad \sinh b_i + \eta_2\Gamma'\lambda_i \cosh b_i + \eta_2 z_{t2}\Gamma'^2\lambda_i^2 \sinh(b_i) \\ -1 \\ 0 \end{bmatrix}$$

where the equation $D_{1i} = -C_{1i}$ arising from equation (7) has been omitted, reducing the dimension of $M(\lambda)$ to 7×7.

The dimensionless parameters ε_l, η_l, ξ_l, α_l, z_{hl}, z_{tl}, z_{mb} which appear in the above matrices are defined in Table 1 which eliminates all dependency upon actual physical parameters from equation (15), with the exception of the elbow angle θ_2. The relatively compact expression obtained for $M(\lambda)$ results from the following additional definitions:

$$\Gamma = \frac{EI_2}{EI_1}, \qquad \Gamma' = \frac{\beta_{2i}}{\beta_{1i}}, \tag{17, 18}$$

$$a_i = \eta\lambda_i, \qquad b_i = \Gamma'(1-\eta)\lambda_i. \tag{19, 20}$$

Clearly from equation (5), when the mass properties EI_l and m_l of the two links are equal, $\Gamma = \Gamma' = 1$. Several additional simplifying expressions are needed to obtain equation (16);

$$\beta_{li}^4 = -s^2 \frac{m_l}{EI_l}, \tag{21}$$

$$\left.\begin{aligned} \frac{I_{hl}s^2}{EI_l\beta_{li}} &= -\varepsilon_l\lambda_i^3 \\ \frac{I_{tl}s^2}{EI_l\beta_{li}^2} &= -\alpha_l\lambda_i^3 \\ \frac{m_{tl}s^2}{EI_l\beta_{li}^3} &= -\eta_l\lambda_i \end{aligned}\right\}. \tag{22}$$

TABLE 1

Dimensionless ratio definitions

Dimensionless ratio	Definition	Description
ε_l	$\frac{I_{hl}}{m_l L^3}$	Hub to beam inertia ratio
η_l	$\frac{m_{tl}}{m_l L}$	Tip mass to beam mass or load ratio
ξ_l	$\frac{k_l L}{EI_l}$	Joint/servo stiffness to beam bending stiffness
α_l	$\frac{(I_{tl} + m_{tl}o_{tl}^2)}{m_l L^3}$	Payload rotary inertia to beam inertia ratio
Z_{hl}	$\frac{o_{hl}}{L}$	Hub offset length ratio
Z_{tl}	$\frac{o_{tl}}{L}$	Tip offset length ratio
Z_{mb}	$\frac{(m_{b2} + m_{t2})}{m_1 L}$	–

The upper left 3×3 partition of $M(\lambda)$, M_{11} is equivalent to the characteristic matrix for a single-link manipulator with the same boundary conditions as the upper link.

An expression for the natural frequencies of the two-link system is obtained from equations (5), (6) and (18) and is given by

$$f_i = \frac{\lambda_i^2}{2\pi L^2}\left(\frac{EI_1}{m_1}\right)^{1/2} = \frac{(\Gamma'\lambda_i)^2}{L^2}\left(\frac{EI_2}{m_2}\right)^{1/2}, \tag{23}$$

where f_i is the resonant frequency corresponding to the system eigenvalue λ_i. Thus, the natural frequencies can be computed in terms of the mass properties of either beam without formulating a dynamic model.

The geometric offsets have two fundamental effects on the eigenvalues: the effective inertia of each tip inertia I_{tl} is increased by $m_{tl}o_{tl}^2$ which increases α_l in Table 1, and extra terms are present in the boundary condition equations (9–14), where the former effect is the most significant. Generally higher modes are more sensitive to inertia and offset terms since the modal slope along the beam increases with mode number and consequently it requires more accurate modelling and parameter determination to accurately predict higher frequencies.

3.3. NUMERICAL SOLUTION METHOD

The differential eigenvalue problem posed is to find non-trivial solutions to equation (15) i.e., the zeros of the characteristic equation defined by,

$$Q(\lambda) = \det\left[M(\lambda, \theta_2, \varepsilon_1, \xi_1, \eta_1, \alpha_1, \eta_2, \alpha_2, \ldots)\right] = 0. \tag{24}$$

For simple systems, such as a single-link, $Q(\lambda)$ can be expressed algebraically. However, even for a simple cantilever, the characteristic equation still requires numerical solution, despite being able to obtain a closed-form expression for $Q(\lambda)$. For the two-link case, $M(\lambda)$ is 8×8 and computing an algebraic expression for the determinant can only be achieved using a symbolic code which would produce a cumbersome expression. Alternately the determinant can be computed numerically and incorporated into the numerical solution for the eigenvalues λ_i. The accuracy of the numerical solution of the transcendental function $Q(\lambda)$ associated with the characteristic equation is validated by Milford [8], where the formulation itself is also validated by reduction to published examples such as those provided by Liu and Huang [14].

The corresponding eigenvectors of equation (15) are obtained by substituting the eigenvalues λ_i into the characteristic matrix M given in equation (16), and computing the eigenvectors of the following eigenvalue problem from equation (15)

$$M\mathbf{v}_i = \psi_i \mathbf{v}_i, \tag{25}$$

where ψ_i are the eigenvalues of $M(\lambda_i)$ which are not the same as the eigenvalues λ_i from the characteristic matrix equation (24). The eigenvectors, $\mathbf{v}_i$, constitute the vector of mode shape constants defined in equation (4) for mode i. This is an alternative to the algebraic solution of the homogeneous simultaneous equations

(15) for the eigenvectors. The normal modes of vibration are defined by substituting λ_i and $\mathbf{v}_i$ into equation (4) with frequency defined in equation (23).

The benefits of this approach can be readily seen. One only needs to formulate the boundary condition expressions (7–14) which can be obtained for an arbitrary number of serial links with arbitrary boundary conditions. The eigenvalues and eigenvectors are obtained numerically without the need for excessive algebraic manipulation. The eigenfunctions will accurately model the true system mode eigenfunctions since the boundary conditions have been rigorously determined.

4. RESULTS

4.1. CONFIGURATION DEPENDENCE OF EIGENVALUES

The effect of the manipulator configuration defined by the elbow angle will now be addressed. In addition to the characteristic function (24) being a non-linear hyperbolic function, it is also a non-linear function of the elbow angle θ_2 which is the source of configuration dependence observed for the modal parameters of a two-link manipulator. Using the numerical values in Table 2, the first three eigenvalues are computed by numerical solution of equation (24) and plotted as a function of elbow angle over a 0–90° range in Figure 3. Clearly the variation in frequency is significant over the 90° elbow angle, with the second mode decreasing by 31·7%. Similar properties have been observed for the space shuttle remote manipulator system (RMS) while executing a large planar manoeuvre [9], where the frequencies vary by as much as 25%. The physical properties of the

TABLE 2

Two-link manipulator parameters

Component	Parameter	Symbol	Units	Upper arm/shoulder	Lower arm/elbow
Beam	Length	L	m	0·500	0·540
	Thickness	–	mm	0·61	0·60
	Width	–	m	0·051	0·051
	Mass	m_b	kg	0·121	0·129
	Stiffness	EI	Nm^2	0·203	0·193
Motor	Hub inertia	I_h	kgm^2	0·0204	0·0088
	Gear ratio	N_g	–	50:1	66:1
	Torque constant	K_m	Nm/A	0·0596	0·0171
	BEMF constant	K_b	V s/rad	0·0573	0·0171
	Armature resistance	R_a	Ω	2·7	3·7
	Viscous friction	c_v	Nm s/rad	7·5e − 5	7·5e − 5
Loads	Tip loads	m_t	kg	0·61	0·224
	Inertia	I_t	kgm^2	1·5e − 3	1·3e − 4
Offsets	Hub offset	o_h	mm	16	37
	Tip offset	o_t	mm	41	20

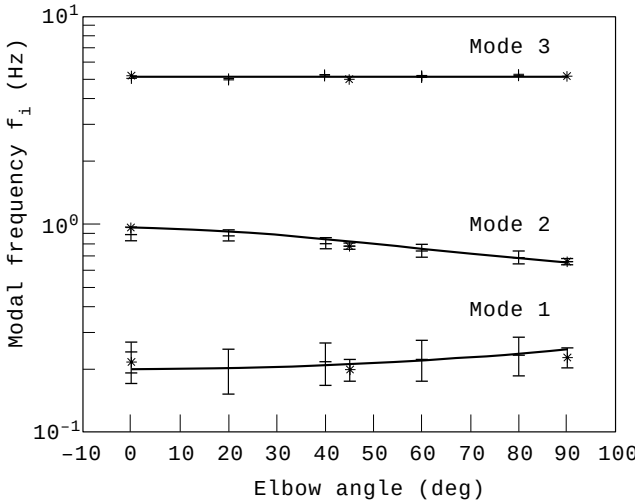

Figure 3. Modal parameter variation with elbow angle. ——, Analytical prediction; ∗, experimental value ($\Delta f = 0{\cdot}049$); +, experimental value ($\Delta f = 0{\cdot}098$).

RMS differ significantly from the manipulator investigated in this paper, however, the degree of flexibility and observed trends are similar.

4.2. EXPERIMENTAL VERIFICATION OF FREQUENCY VARIATION WITH ELBOW ANGLE

The experimental manipulator shown in Figure 4 [8] was used to verify the analytical results presented in the previous section. The manipulator comprises two flexible links driven by two DC servo-motors with parameters defined in

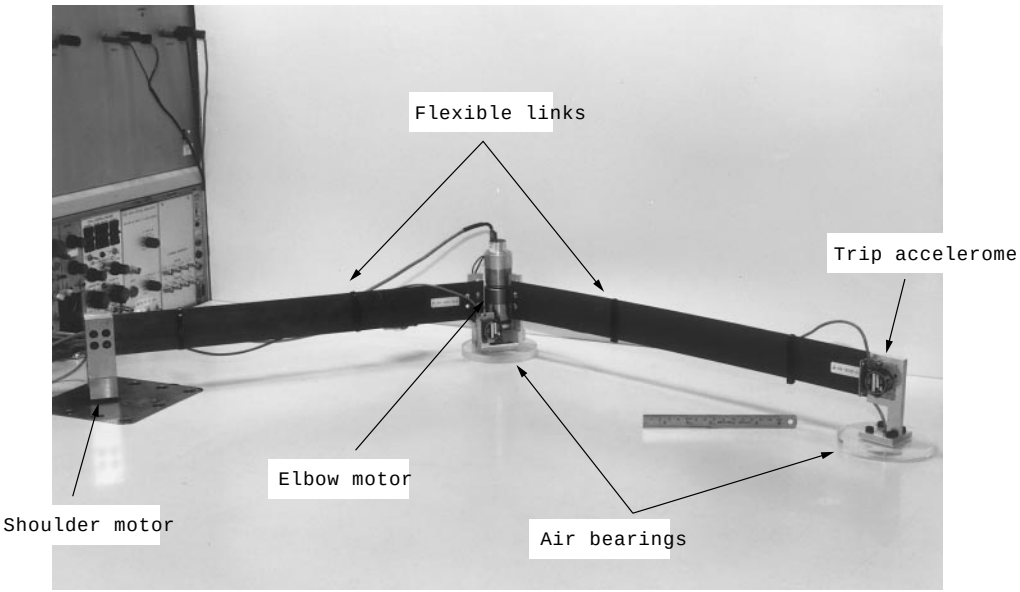

Figure 4. Experimental two-link flexible manipulator.

Figure 1 and Table 2. Vibration is sensed by a tip mounted accelerometer for system identification purposes.

Frequency domain system identification methods were used to obtain eigenfrequencies for several discrete elbow angles. At each elbow angle the manipulator was excited by applying a band-limited white noise input voltage to the shoulder servo-motor. A transfer function estimate was computed from the input excitation voltage and measured tip acceleration [15]. The first three natural frequencies extracted from the transfer function estimate are plotted in Figure 3, along with those predicted by the mathematical model. The error bars denote the resolution of the frequency spectrum available during the system identification procedure, which is a conservative upper bound on the accuracy of the identified eigenfrequencies; two separate sets of data are presented, corresponding to frequency resolutions of 0·049 and 0·098 Hz, respectively. Clearly the theoretical results accurately predict the experimentally observed variation in frequency for the three modes shown. In particular, the large variation in mode 2 is predicted with an accuracy of approximately 2·2%.

5. CONCLUSIONS

A system mode solution to the PDE was derived for a general two-link manipulator, extending the method presented by Oakley [10]. By correctly modelling the shear force and bending moment at the elbow joint and including geometric offsets, solution of the characteristic equation produced true system mode eigenfrequencies without recourse to a dynamic formulation. A numerical solution approach was developed for the high order eigenvalue problem resulting from the system mode formulation. The analysis was subsequently shown to accurately predict the modal frequency variations with elbow angle observed experimentally for the two-link manipulator.

The eigenfrequencies vary by up to 30% over a 90° elbow angle, which is sufficient to challenge the robustness of a fixed gain controller. In related research, the authors incorporate the modal analysis techniques presented in this paper into dynamic models for synthesis of fixed gain [8] and gain scheduled [15] vibration compensators.

REFERENCES

1. J. L. Junkins and Y. Kim 1993 *Introduction to Dynamics and Control of Flexible Structures*. Washington: AIAA.
2. R. D. Blevins 1979 *Formulas for Natural Frequency and Mode Shape*. New York: Van Nostrand Reinhold.
3. E. Schmitz 1985 *Ph.D. Thesis*, *Department of Aeronautics and Astronautics*, *Stanford University*. Experiments on the end-point position control of a very flexible one-link manipulator.
4. S. Yurkovich, U. Ozguner, A. Tzes and P. T. Kotnik 1987 in *Proceedings of the Workshop on Space Telerobotics*, JPL Publication 87-13, **III**, 279–288. Flexible manipulator control experiments and analysis.

5. E. Barbieri and U. Ozguner 1988 *Journal of Dynamic Systems, Measurement, and Control* **110**, 416–421. Unconstrained and constrained mode expansions for a flexible slewing link.
6. E. Garcia and D. J. Inman 1991 *Journal of Guidance, Control, and Dynamics* **14**, 736–742. Modeling of the slewing control of a flexible structure.
7. C. M. Oakley and R. H. Cannon Jr. 1989 in *Proceedings of the First International Symposium on Experimental Robotics, Montreal, Canada*. Theory and experiments in selecting mode shapes for two-link flexible manipulators.
8. R. I. Milford 1994 *Ph.D. Thesis, Department of Mechanical Engineering, University of Queensland, Australia*. Experimental frequency domain identification and adaptive control of a flexible two-link robot manipulator.
9. M. A. Scott, M. G. Gilbert and M. E. Demeo 1993 *Journal of Guidance, Control, and Dynamics* **16**, 275–280. Active vibration damping of the space shuttle remote manipulator system.
10. C. M. Oakley 1991 *Ph.D. Thesis, Department of Mechanical Engineering, Stanford University*. Experiments in modelling and end-point control of two-link flexible manipulators.
11. A. Rutenberg 1978 *Journal of Applied Mechanics* **45**, 422–423. Vibration frequencies for a uniform cantilever with a rotational constraint at a point.
12. S. Thompson 1989 *Control Systems, Engineering and Design*. London: Longman. See pp. 237–334.
13. T. W. Lee 1973 *Journal of Applied Mechanics*, September, 813–815. Vibration frequencies for a uniform beam with one end spring-hinged and carrying a mass at the other free end.
14. W. H. Liu and C. C. Huang 1988 *Sound and Vibration* **123**, 31–42. Free vibration of restrained beam carrying concentrated masses.
15. R. I. Milford and S. F. Asokanthan 1995 in *Proceedings of the* 1995 *American Controls Conference, Seattle, WA*. Identification and gain scheduled control of an experimental two-link flexible manipulator.

APPENDIX: DC SERVO ACTUATOR BOUNDARY CONDITION MODELLING

Each joint of the manipulator in Figure 1 is powered by a DC servo-motor. Considering a single actuator/beam pair in isolation, the servo powered joint contributes increased hub inertia and viscous friction, and adds a control gain dependent electromechanical stiffness to the dynamics of the flexible structure. Consideration of these effects is required to accurately model the boundary conditions for solution of the PDEs. The equivalent stiffness of the servo-motor under closed-loop feedback, when modelled as a torsional spring boundary condition for the flexible beam is determined by both its mechanical stiffness and the electromechanical controller stiffness. Given the relatively high stiffness of commercial gear trains, the combined or resultant stiffness is dominated by the servo torque. The relation between the control law and the equivalent stiffness is developed in this Appendix, where we shall demonstrate that a high gain servo loop produces the locked elbow boundary condition assumed in section 3.

The linear dynamics for an armature controlled DC servo-motor are developed from the model in Figure A1 which is segmented into motor, gearbox and load components where the latter is the manipulator link driven by the servo. Neglecting inductance L_a, Coulomb friction and backlash, the electromechanical

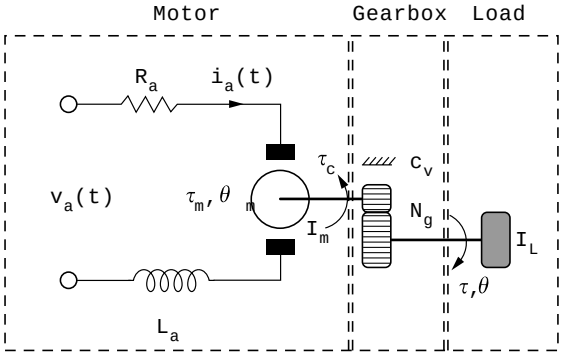

Figure A1. DC servo-motor schematic.

torque applied by the gearbox output shaft to the load contributed by the flexible beam I_L is [6, 8],

$$\tau(s) = \frac{N_g K_m}{R_a} v_a(s) - N_g^2 \left(\frac{K_m K_b}{R_a} + c_v \right) \dot{\theta}(s) - I_m N_g^2 \ddot{\theta}(s), \tag{A1}$$

where N_g is the gear ratio ($N_g \geqslant 1$), θ is the gearbox output shaft angle, K_m is the motor gain constant, v_a is the applied armature voltage, K_b is the back EMF (BEMF) constant, R_a is the armature resistance, I_m is the inertia of the motor shaft and c_v is the total viscous friction of the joint. The subscript "a" denotes armature circuit quantities while the subscript "m" designates the motor side of the gearbox.

The armature voltage v_a derived from closed-loop position control is approximated by the proportional feedback control law

$$v_a(k) = K_P e(k), \tag{A2}$$

where $e(k) = \theta^d(k) - \theta(k)$ is the joint angle error while tracking the target trajectory $\theta^d(k)$ and K_P is the proportional feedback gain. The equivalent stiffness of the servo relative to the gearbox output under closed-loop proportional feedback control is computed from equations (A1) and (A2) and defined by

$$k = \left. \frac{\tau(s)}{e(s)} \right|_{s=0} = \frac{N_g K_m K_P}{R_a}. \tag{A3}$$

This active *servo stiffness* definition is independent of the inertia and the passive stiffness of the servo; it is determined by the control law which can be designed to be of sufficiently high bandwidth to constitute a clamped boundary condition neglecting backlash and the mechanical stiffness of the support structure. In fact, it is probable that the servo bandwidth will be high in most applications to enable high bandwidth hub trajectory tracking, and hence the servo stiffness can usually be assumed to be constant for the modal analysis. This ability to partially "control" the boundary condition of the beam is a useful result which reduces the modelling uncertainty (see, e.g., reference [6]) provided that sufficient control authority exists to enforce this condition.

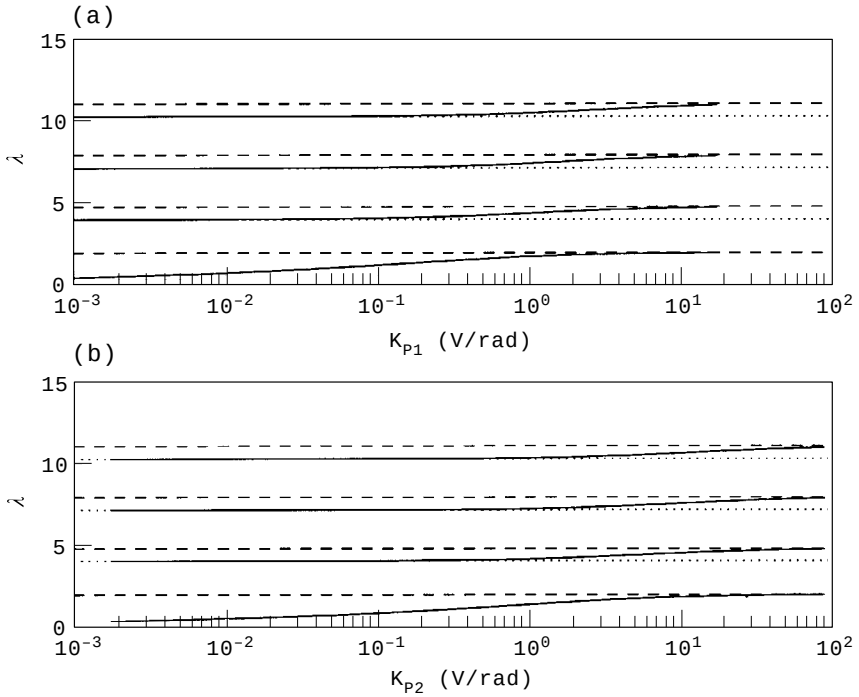

Figure A2. Spring-hinged boundary condition. The eigenvalues are shown versus the servo proportional gain K_P for both joints. The eigenvalues for the standard cases are also shown for reference: – – –, clamped–free; · · · · ·, pinned–free. (a) Shoulder servo; (b) elbow servo.

It is convenient to relate the proportional gain to the equivalent dimensionless spring stiffness parameter ξ. The proportional gain corresponding to ξ from equation (A3) and Table 1 is

$$K_{Pl} = \frac{EI_l R_{al}}{LN_{gl} K_{ml}} \xi_l, \qquad l = 1, 2, \tag{A4}$$

where the link subscript l has been added for generality.

Treating the two links independently, from equation (A4) the first four eigenvalues are plotted against K_{pl} in Figure A2. The proportional gain which yields a near clamped boundary condition ($\xi = 50$) is $K_P \approx 8{\cdot}7$ V/rad for the shoulder and 43·9 V/rad for the elbow servo, using the parameters given in Table 2. We can also observe that the sensitivity to K_P decreases with mode number. In practice, friction also contributes to the boundary condition enabling a lower value of K_P to achieve the same result.